Research Article

For reprint orders, please contact: reprints@futuremedicine.com

Nanomedicine

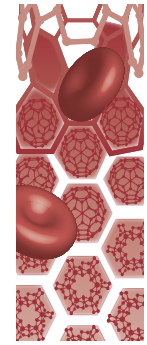

Ultra-small solid archaeolipid nanoparticles for active targeting to macrophages of the inflamed mucosa

Aim: Develop nanoparticulate agents for oral targeted delivery of dexamethasone (Dex) to macrophages of inflamed mucosa. **Materials & methods:** Solid archaeolipid nanoparticles (SAN-Dex) (compritol/*Halorubrum tebenquichense* polar archaeolipids/soybean phosphatidylcholine/Tween-80 4; 0.9; 0.3; 3% w/w) loaded with Dex were prepared. Their mucopenetration, stability under digestion and *in vitro* anti-inflammatory activity, were determined. **Results:** Ultra-small SAN-Dex strongly reduced the levels of TNF-α, IL-6 and IL-12 on J774A1 cells stimulated with lipopolysaccharides as compared with free Dex or loaded in ordinary solid lipid nanoparticles-Dex. After *in vitro* digestion, the anti-inflammatory activity of SAN-Dex was retained, while that of solid lipid nanoparticles-Dex was lost. **Conclusion**: Because of their structural and pharmacodynamic features, SAN-Dex may be suitable for oral targeted delivery to inflamed mucosa.

First draft submitted: 30 December 2016; Accepted for publication: 3 March 2017; Published online: 27 April 2017

Keywords: digestion stability • inflammatory bowel disease • oral delivery

Leticia Herminia Higa[1], Horacio Emanuel Jerez[1], Marcelo Alexandre de Farias[2], Rodrigo Villares Portugal[2], Eder Lilia Romero[1] & Maria Jose Morilla*[,1]

[1]Nanomedicine Research Program, Departamento de Ciencia y Tecnología, Universidad Nacional de Quilmes, Roque Saenz Peña 352, Bernal, B1876BXD, Argentina

[2]Brazilian Nanotechnology National Laboratory, CNPEM, Caixa Postal 6192, CEP 13.083–970, Campinas, São Paulo, Brazil

*Author for correspondence:
Tel.: +54 1143657100
Fax: +54 1143657132
jmorilla@unq.edu.ar

Inflammatory bowel diseases (IBD) such as Crohn's disease and ulcerative colitis, are incurable relapsing disorders of the GI tract (GIT), characterized by chronic inflammation and epithelial injury induced by the uncontrolled activation of the mucosal immune system [1,2]. Seventy percent of IBD patients experiencing more aggressive symptoms will require at least one surgical intervention during lifetime [3,4]. The treatment of IBD is symptomatic, and depending on the stage of the disease, ranges from oral aminosalicylates, anti-inflammatory and immunosuppressant drugs, to endovenous or subcutaneous biological agents such as the anti-TNF-α antibodies infliximab or adalimumab, and certolizumab pegol, respectively [5,6]. Conventional treatments have limited benefits, because of their systemic adverse effects displayed during the long-term use [7]. Despite the quick advance of biological therapies for IBD treatment, a third of Crohn's disease patients fail to respond to anti-TNF-α and many lose response over time [8,9]. Additionally, the biological approach is highly expensive and has increased risks of opportunistic infections, autoimmunity, infusion reactions and lymphoma [10,11].

Oral corticosteroids are a typical example of a long-term treatment expected to display adverse systemic side effects [12]. Antibodies, despite their recognized selectivity, have shown undesirable activity on tissues expressing the target receptor [13]. Overall, drugs used for IBD treatment are systemically distributed, not site specific delivered. Counting on oral site specific targeted delivered treatments, besides making use of a compliant route of administration for patients, may significantly reduce the side effects and improve the outcome of long-term current treatments.

Chronicity of IBD results from uncontrolled activity of mucosal immune cells,

Future Medicine part of fsg

such as macrophages, T cells and subsets of innate lymphoid cells [14]. Following activation, which occurs in response to components of the commensal microbiota and pattern recognition receptors signaling such as toll-like receptors and nucleotide-binding oligomerization domains, macrophages and dendritic cells produce large amounts of proinflammatory cytokines, such as IL-1β, IL-6, IL-8 and TNF-α. The imbalance between proinflammatory and anti-inflammatory cytokines impedes the resolution of inflammation, leading to disease perpetuation and tissue destruction [15]. Delivering anti-inflammatory drugs to macrophages and dendritic cells with targeted nanoparticles could make IBD treatments more efficient.

The therapeutic success of oral targeted nanoparticles, however, depends on its capacity to remain structurally stable along the GI transit, and on the feasibility of accessing the target cells. If well, the GIT is the most hostile environment in the organism, the differences between inflamed mucosa of IBD patients and the normal gut, can be exploited for nanoparticle-mediated targeted delivery. Examples of this are the loss of the inner adherent and the outer mobile mucus layer; the infiltration of immune cells such as neutrophils, macrophages, lymphocytes and dendritic cells [16]; the accumulation of positively charged proteins such as transferrin [17], bactericidal/permeability-increasing protein, and antimicrobial proteins [18,19]; and the disruption of the epithelial barrier function with the concomitant increase of permeability of the inflamed mucosa [20]. In this pathological context, macrophages can be found at the luminal side of the inflamed mucosa, favoring its accessibility from the oral route. On the other hand, the local pH is decreased (from 6.8 to 7.2 in normal mucosa to 5.5 to 2.3 in IBD patients' mucosa [21]) and the GI transit is enhanced, with frequent diarrhea. Overall, in order to reach mucosal macrophages in an intact form, oral nanoparticles have to overcome extremely low pHs, the activity of degradative enzymes, and avoid to be trapped within the mucus layer during the transit across the healthy portions of the gut. Additionally, negatively charged and small sized nanoparticles have been reported to accumulate in high extent into the inflamed mucosa [22].

Here we report the development of ultra-small, negatively charged solid archaeolipid nanoparticles (SAN), for oral targeted delivery of dexamethasone (Dex) to macrophages. SAN have a solid lipid core of compritol, covered by a protective shell of total polar archaeolipids (TPA) extracted from the hyper halophilic archaebacteria *Halorubrum tebenquichense*. TPA are a mixture of saturated isoprenoid chains linked via ether bonds to the glycerol carbons at the *sn* 2,3 position. On the one hand, in contrast to phospholipids, TPA are resistant against lipolytic enzymes, hydrolytic and oxidative attacks [23]. On the other hand, TPA are ligands for scavenger receptors class A [24] highly expressed on macrophages and dendritic cell. Our hypothesis is that SAN, by combining high structural endurance against destructive agents in the GIT with extensive macrophages uptake may be well suited for oral targeted delivery to the inflamed mucosa.

Materials & methods

Materials

Compritol ATO 888 (Compritol) was a gift from Daltosur SRL (Gattefosse). Soybean phosphatidylcholine (SPC, purity >90%) was a gift from Lipoid, Ludwigshafen, Germany. Dexamethasone (Dex), 3-(4,5-dimethylthiazol-2-yl)-2,5-diphenyl tetrazolium bromide (MTT), lipopolysaccharides from *Escherichia coli* 0111:B4 (LPS), pepsine, mucin type III porcine extracted from stomach and 3-(2′-benzothiazolyl)-7-diethylaminocoumarin (coumarin-6, C6) were from Sigma-Aldrich (MO, USA). Tween 80 (T80) was acquired from Merck. Porcine pancreatic lipase was a gift from Gador (Biozym). Roswell Park Memorial Institute 1640, Dulbecco's Modified Eagle Medium, penicillin-streptomycin sulphate, glutamine, sodium pyruvate and trypsin/ethylenediamine tetra acetic acid were from Gibco®, Life Technologies (NY, USA), fetal bovine serum was from Internegocios, Cordoba, Argentina. The other reagents were of analytic grade from Anedra, Research AG (Buenos Aires, Argentina).

Archaebacteria growth, extraction & characterization of TPA

Halorubrum tebenquichense archaea, isolated from soil samples of Salina Chica, Peninsula de Valdés, Chubut, Argentina were grown in basal medium supplemented with yeast extract and glucose at 37°C [25]. Biomass was grown in 15-l medium in a 25-l home-made stainless steel bioreactor and harvested after 96-h growth. TPA were extracted from biomass using the Bligh and Dyer method modified for extreme halophiles [26]. Between 400 and 700 mg TPA were isolated from each culture batch. The reproducibility of each TPA-extract composition was routinely screened by phosphate content [27] and electrospray-ionization mass spectrometry, as described in [28].

Preparation & characterization of solid lipid nanoparticles

Ordinary solid lipid nanoparticles (SLN) made of compritol: SPC: T80 at 4: 1.2: 3% w/w and SAN

made of compritol: TPA: SPC:T80 at 4: 0.3: 0.9: 3% w/w) (SAN25), 4: 0.6: 0.6: 3%w/w (SAN50), 4: 0.9: 0.3: 3 w/w (SAN75) and 4: 1.2: 0: 3 w/w (SAN100) were prepared by the emulsion-ultrasonication method [29]. To that aim in one test tube 120 mg compritol (oil phase) were melted at 75–80°C in a water bath. In another separate tube, SPC (36, 27, 18, 9 and 0 mg), TPA (0, 9, 18, 27, 36 mg) and T80 (90 mg) were suspended in 3 ml of ultra-pure water and heated at the same temperature as compritol. The aqueous phase was homogenized for 30 s using an Ultra Turrax T10 Basic (IKA, Germany) and immediately added dropwise into the oil phase under homogenization at 13,000 r.p.m. at 75–80°C. This hot oil-in-water emulsion was sonicated with a probe-type sonicator (6 mm probe, Sonics & Materials, Inc., Vibra Cell Power, USA, 130 Watt), at 70% amplitude for 10 min. In order to obtain a nanoparticle suspension, the nano-emulsion was cooled down at 4°C.

To prepare Dex-loaded nanoparticles (SLN-Dex and SAN-Dex) 2, 5 or 10 mg Dex were mixed with 120 mg compritol (oil phase at 0.6; 1.66 or 3.3% w/w, respectively) and processed as stated before. After solidification, nanoparticles were filtrated across a nylon syringe filter membrane of 1.2 µm pore size to eliminate free Dex.

To prepare C-6 labeled nanoparticles (SLN-C6 and SAN-C6), 0.3 mg of C6 (0.1% w/w) were mixed with 120 mg compritol and processed as stated before.

Size & ζ potential

Size and ζ potential of nanoparticles were determined by dynamic light scattering and phase analysis light scattering, respectively, using a Zeta nanosizer equipment (Malvern Instruments, Malvern, UK).

Quantification of dexamethasone

Dex was quantified by spectrophotometry at 243 nm after complete disruption of 20 µl of nanoparticles suspension in 3 ml $CHCl_3$:CH_3OH (9:1 v/v). Void nanoparticles were used as blank. The absorbance of the sample was compared with a standard curve prepared with Dex in $CHCl_3$:CH_3OH (9:1 v/v). The standard curve was linear in the range 0–30 µg/ml with correlation coefficient of 0.99. The encapsulation efficiency (% EE) of the Dex-loaded nanoparticles was calculated using the following relationship: %EE = (amount of drug in the filtrated/amount of drug added) × 100.

Quantification of coumarin-6

C6 was quantified spectrofluorometric (λ_{Ex} 465 nm and λ_{Em}490 nm) after complete disruption of one volume of nanoparticles in 7000 volumes of CH_3CH_2OH. The fluorescence intensity of the sample was compared with a standard curve prepared with C6 in $CHCl_3$ or CH_3CH_2OH. The standard curve was linear in the range 0.05–20 ng/ml with correlation coefficient of 0.991.

Morphology

The morphology of nanoparticles was studied by transmission electron microscopy (TEM) and cryo-TEM.

TEM

Aqueous suspensions of nanoparticles were deposited on a carbon grid membrane and the grid covered with a drop of phosphotungstic (2% w/v). Then, the grids were air-dried and analyzed using a Jeol 1200-EX II (Tokyo, Japan) instrument.

Cryo-TEM

Samples were prepared in a controlled environment vitrification system (Vitrobot Mark I, FEI, The Netherlands) with controlled temperature (22°C) and humidity (100%). Samples were examined in Jeol JEM-1400Plus (JEOL, Japan) instrument, operating at 120 kV. Image collections were made using a CCD camera Gatan Multi Scan 794. Images were not processed after acquisition. Sample preparation and data acquisition were performed at the Electron Microscopy Laboratory (LME)/Brazilian Nanotechnology National Laboratory (LNNano).

Thermal analysis

Calorimetric analysis of the solid bulk materials (drug and lipids) and of aqueous suspension of nanoparticles were performed using a Differential scanning calorimetry (DSC) Q200 TA instrument equipped with a *Refrigerator Cooling System* (RCS90). Briefly, 3–5 mg of suspension of nanoparticles was taken in an aluminium pan. DSC scans were recorded from -50 to 90°C for aqueous suspensions and from -50 to 290°C for bulk material at a heating rate of 10°C/min, using an empty pan as reference. Melting point and enthalpy were calculated using the software TA Universal analysis provided by TA Instruments®. The index of recrystallization (R.I.) was calculated according to the following equation: R.I.(%) = ΔH nanoparticles dispersion (J/g)/[ΔH bulk material (J/g) × concentration lipid phase (%)] × 100

Interaction of nanoparticles with mucin

Change in size

The aggregation of nanoparticles in contact with mucins was measured in terms of size, polydispersity index (PDI), ζ potential and absorbance at 650 nm as described in Supplementary Material.

Diffusion study

The diffusion of nanoparticles across a mucus layer was measured using the Transwell system as described in the Supplementary Material.

Cell lines & culture

Immortalized murine macrophages J774A.1 (ATCC® TIB-67™) were supplied by Dra. Erina Petrera, Facultad de Ciencias Exactas y Naturales, Universidad Nacional de Buenos Aires, Argentina. Caco-2 cells were kindly provided by Dr Osvaldo Zabal, INTA Castelar, Buenos Aires, Argentina.

J774A.1 cells were maintained in RPMI 1640 and Caco-2 cells were maintained in Dulbecco's Modified Eagle Medium with 1% pyruvate, both were supplemented with 10% fetal bovine serum, 100 U/ml penicillin 100 µg/ml streptomycin and 2 mM L-glutamine and were grown in a humidified atmosphere of 5% CO_2 at 37°C.

Cell viability

The viability of J774A.1 and Caco-2 cells upon 24-h incubation with void and Dex-loaded nanoparticles was measured by the MTT assay as described in Supplementary Material.

Cellular uptake

The uptake of C6-labeled nanoparticles by macrophages and enterocytes was measured in the absence and presence of a mucin layer (275 µg mucin; 0.5 mg/ml) by flow cytometry. Briefly, J774A.1 and Caco-2 cells were seeded on 24-well culture plates at a density of 1.5×10^5 cells per well and grown for 24 h. Then, cells were incubated with 40 µg/ml SLN-C6 and SAN-C6 in complete medium for different time periods (1, 3 and 5 h) at 37 and 4°C (as a control to determine the unspecific adsorption on cell surface). After incubation, the cells were trypsinized, washed with phosphate-buffered saline and a total of 1×10^4 cells were analyzed by flow cytometry (BD FACSCalibur™; BD Biosciences, CA, USA). Data were analyzed using WinMDI 2.9 software (Microsoft, WA, USA). The fluorescence was further normalized to the C-6 content of each formulation.

Stability under gastrointestinal conditions

Colloidal stability in simulated gastric fluid

To assess for the structural stability of nanoparticles, and their potential aggregation into the GIT, a simulated gastric fluid (SGF), which comprised 3.2 mg/ml pepsin, 34.2 mM NaCl at pH 1.2 were prepared. Then, 0.1 ml of nanoparticles were diluted with 0.9 ml of SGF and incubated at 37°C during 4 h. Then samples were centrifuged for 10 min at 10,000 r.p.m. to remove pancreatic aggregates from the fluid. The particle size and ζ potential after incubation were determined as stated above.

In vitro lipolysis

The assessment *of in vitro* lipolysis of nanoparticles was performed under simulated fasted-state intestinal fluid (SIF), according to Porter and Charman [30] with minor modifications. Briefly, 300 µl of nanoparticles were added into 3 ml of digestive medium comprising 150 mM NaCl, 5 mM $CaCl_2$, 5 mM sodium taurocholate, 1.25 mM lecithin, 300 IU/ml porcine pancreatic lipase and 0.5% SDS buffered at pH 6.8 with Tris-HCl 10 mM. The mixture was incubated in a thermostatic water bath at 37°C. The pH was maintained at 6.8 throughout the whole lipolysis process by manual titration with 0.2 M NaOH to neutralize the fatty acid produced by the digestion of lipids. The digestion process was considered complete when the pH change was less than 0.05 units within a 15-min interval. Cumulative lipolysis percentage versus time profiles of nanoparticles titrated with NaOH were plotted.

In vitro anti-inflammatory activity

The *in vitro* anti-inflammatory activity of Dex-loaded nanoparticles was determined by measuring the release of proinflammatory cytokines by cells stimulated with LPS. Briefly, J774.A1 were seeded at a density of 2×10^5 cells per well onto 24-well plates and grown for 24 h at 37°C. Then cells were co-incubated with 1 µg/ml LPS and void nanoparticles at 40 µg/ml Compritol, Dex-loaded nanoparticles at 40 µg/ml Compritol-10 µg/ml Dex and Dex-loaded nanoparticles previously submitted to a digestion process. Briefly, 0.1 ml of nanoparticles were incubated with 0.9 ml of SGF at 37°C for 30 min in an orbital shaker. After that, pH was adjusted to 6.8 using 1 M $NaHCO_3$. Then 1 ml of SIF was added and incubated along 2 h. These digested nanoparticles were used for co-incubation. LPS-stimulated and nonstimulated cells without treatments were used as positive and negative controls, respectively. After 24 h of incubation at 37°C, supernatants were collected and stored at -20°C until analysis.

Mouse TNF-α, IL-12 and IL-6 levels were measured by enzyme-linked immune sorbent assay (BD OptEIA™, BD Biosciences) following the manufacturer's instructions. Absorbance measurements were carried out at 450 nm on a microplate reader in a microplate reader.

Stability upon storage

The colloidal stability of aqueous suspension of nanoparticles and drug content were determined after 6 months stored at 4°C. Nanoparticle size, ζ potential

and Dex quantification before and after storage were determined as stated before.

Statistical analysis

Statistical analyses were performed by one-way analysis of variance followed by Dunnet's or Turkey test using Prisma 4.0 Software (Graph Pad, CA, USA). p-value of <0.05 was considered statistically significant. *p < 0.05; **p < 0.01; ***p < 0.001; ****p < 0.0001; n.s. represents not significant (p > 0.05).

Results

Preparation & characterization of SAN containing dexamethasone

Four different formulations were prepared derived from ordinary SLN made of compritol: SPC: T80 (4:1.2:3% w/w), replacing SPC by increasing amounts of TPA (25, 50, 75 and 100% weight), to obtain the so-called SAN (SAN25, SAN50, SAN75 and SAN100, respectively).

We have observed that the replacement of SPC by TPA roughly reduced by threefold the nanoparticle size (~300 and ~100 nm). Besides, the presence of TPA reduced the PDI values from 0.42 to approximately 0.3 and the ζ potential from -8 to -30–40 mV (Supplementary Table 1).

Due to the high content of TPA, minimum size (<100 nm), low PDI value and negative ζ potential, SAN75 was chosen to be loaded with dexamethasone (from this point on we will call them SAN).

Structural features of Dex-loaded nanoparticles are shown in Table 1. The EE was highest for 5 mg of Dex, resulting 48.5 ± 18.4% and 59.6 ± 9.7% for SAN-Dex and SLN-Dex, respectively. When loaded into SAN and SLN the intrinsic solubility of Dex (71 ± 12 µg/ml) was increased by 11.2- and 13.9-fold, respectively. Dex incorporation did not cause significant changes in size, PDI and ζ potential respect to void nanoparticles. Both types of nanoparticles, SLN and SAN, have encapsulated threefold more Dex than SLN made of stearic acid, SPC and poloxamer 0.5: 0.5: 0.5 w/w (235 µg/ml Dex) prepared by hot microemulsion technique [31].

Morphology of SAN and SLN was analyzed by TEM and cryo-TEM. TEM images of SLN (Supplementary Figure 1A) and SAN (Supplementary Figure 1C) showed spherical nanoparticles of roughly 100 nm mean diameter. Cryo-TEM images of SLN presented high amount of very large structures of low electron density and few small structures (e.g., needles) of high electron density (Supplementary Figure 1B). The SAN presented small structures of high electron density similar to those observed in SLN (Supplementary Figure 1D). Although larger structures of low electron density were also observed in SAN, these structures differed from those observed in SLN. In SAN, the low electron density structures (50–100 nm) were dominant and could be interpreted as different projection of the high electron density structure. This morphology is typical of formation of very anisometric, platelet-shaped nanoparticles upon crystallization of spherical triglyceride nanodroplets after processing [32,33]. Depending on the angle of observation in the vitrified sample, these particles may appear as circular, ellipsoidal or elongated edged structures (top-view on the platelets) or as needle-like structures of higher contrast (platelets viewed edge-on) [34].

DSC analysis showed a 3.3°C reduction on the melting point of compritol for SAN, SLN and SLN-Dex (Supplementary Table 2). For SAN-Dex the reduction was 7.8°C. This is in agreement with previous data, where the small size of the lipid core, the increment of the superficial area and the presence of surfactant in the melted lipid, are reported to cause a reduction on the melting point of the solid lipid [35]. On the other hand, the endothermic peak of Dex was absent in SAN-Dex and SLN-Dex thermograms, meaning that the major proportion of Dex was dissolved into the lipid matrix in amorphous state, as already reported [36]. Crystallinity of compritol into nanoparticles remained unchanged as no significant changes in R.I. have been observed.

Interaction of nanoparticles with mucins

Mucoadhesive nanoparticles, of big size, highly positive or with hydrophobic surfaces, show great interaction with mucus and keep retained in mucins [37]. This interaction leads to the fast elimination of nanoparticles reducing their access to the epithelium surface. Opposing, mucus penetrating nanoparticles, of small size, negatively or with hydrophilic surface, penetrate the mucus layer and could access to the underlining epithelium. The interaction of SAN and SLN with a mucin layer, in terms of change in mean size (mucoadhesion) and diffusion (mucus penetration) was therefore determined.

In the first place, we found that both, SAN and SLN, were not mucoadhesive: if well the size distribution of SAN becomes broader upon 4 h of incubation with mucins, the size distribution of the nanoparticles/mucin mixtures is in the same size range of nanoparticles alone (Supplementary Figure 2). There were, however, changes in the intensity of the peak, implying that there may be a small fraction of nanoparticles bound to the mucins.

In second place, we found that SAN were more mucus penetrating than SLN: upon 4 h, SAN diffused significantly more (95 ± 2%) than SLN (75 ± 3%) through a mucin layer.

Table 1. Characterization of Dex- and Coumarin 6-loaded nanoparticles.

Formulation	Mean diameter (nm)	PDI	ζ potential (mV)	Dex (μg/ml) or Coumarin 6 (μg/ml)	Encapsulation efficiency (%)
SLN-Dex	278 ± 61	0.37 ± 0.12	-15 ± 2	992 ± 155	59.6 ± 9.7
SAN-Dex	67 ± 18	0.40 ± 0.02	-41 ± 2	807 ± 295	48.5 ± 18.4
SLN-C6	267 ± 44	0.30 ± 0.12	-13 ± 1	140 ± 13	100 ± 30
SAN-C6	91 ± 8.0	0.51 ± 0.04	-38 ± 7	73 ± 6	71 ± 12
SLN-Dex (6)	336 ± 25	0.36 ± 0.11	-10 ± 2	528 ± 130	–
SAN-Dex (6)	77 ± 16	0.43 ± 0.03	-29 ± 4	744 ± 57	–

Data are expressed as mean ± standard deviation (SD) from three independent batches.
Dex: Dexamethasone; PDI: Polydispersity index; SAN: Solid archaeolipid nanoparticle; SLN: Solid lipid nanoparticle; SLN-C6 and SAN-C6: Coumarin 6 loaded SLN and SAN, respectively; SLN-Dex and SAN-Dex: Dexamethasone-loaded SLN and SAN, respectively; SLN-Dex (6) and SAN-Dex (6): Dexamethasone-loaded SLN and SAN upon 6-month storage at 4°C.

Cell viability

In Supplementary Figure 3, the viability of J774A.1 and Caco-2 cells after 24-h incubation with void and Dex-loaded nanoparticles, as determined by MTT, is shown. It was found that the viability of J774A.1 cells and Caco-2 cells did not significantly decrease upon incubation with void or Dex-loaded SAN between 400 and 40 μg/ml of compritol after 24 h. A higher compritol concentration (4000 μg/ml), led to a more significant viability loss of 75%. Similar results were obtained for Caco-2 cells incubated with void and Dex-loaded SLN, in contrast viability of J774A.1 cells incubated with SLN at 400 μg/ml decreased.

Same results were shown for SAN25, SAN50 and SAN100, indicating that toxicity is related to the lipid core and not to the presence of TPA. Surprisingly, for SAN at 400 μg/ml viability increases with increasing concentration of TPA.

Cellular uptake

In Figure 1, the uptake of C6-labeled nanoparticles by J774 A.1 and Caco-2 cells, as measured by flow cytometry along 5 h in the absence and presence of a mucin layer, is shown. In both cell types, the extent of uptake was higher for SAN than for SLN. The absolute amount of uptake was the highest for J774 A.1 cells. At 5 h, uptake by J774 A.1 cells was sixfold higher for SAN-C6 than for SLN-C6, while uptake by Caco-2 cells was 2.4-fold higher for SAN-C6 than for SLN-C6. In both cell types, the extent of uptake was decreased in the presence of a mucin layer (2.75 mg), being almost negligible by Caco-2 cells but remaining high for SAN by J774A.1 cells.

Stability under gastrointestinal conditions

Stability of nanoparticles incubated in SGF and SIF, was determined in terms of size retention and lipolytic percentage, respectively. Neither SLN nor SAN revealed a modification in the particle size or ζ potential upon 4 h of incubation in SGF with respect to initial time. Lipolysis of SLN was relatively fast, being almost completely digested in 30 min (Supplementary Figure 4). In contrast, the lipolysis was significantly lower for SAN, up to 60 min the accumulative lipolytic percentage was 45%.

Anti-inflammatory effect of nanoparticles on macrophages stimulated with LPS

The effect of Dex containing nanoparticles on proinflammatory cytokines levels was determined after cellular incubation with 1 μg/ml LPS in culture media for 24 h. In Figure 2 the levels of IL-6, TNF-α and IL-12 induced on J774A.1 cells are shown. While free Dex did not reduce the TNF-α and IL-12 and only reduced the IL-6 titers (75%), SLN-Dex reduced the IL-6 and IL-12 levels (25 and 75%, respectively). SAN-Dex was the formulation inducing the most pronounced decrease in the three cytokine levels (50% of TNF-α, 75% of IL-6 and 33% of IL-12). Void nanoparticles did not affect the cytokine levels. Remarkably, after being submitted to *in vitro* digestion, SLN-Dex lost the capacity to reduce IL-12, in contrast SAN-Dex retained the capacity to reduce the cytokine levels.

Stability of nanoparticles upon storage

The size and Dex content of freshly prepared and stored for 6 months at 4°C nanoparticles were determined. We observed that after 6 months the size and PDI of both types of nanoparticles remained unchanged but SAN-Dex retained more Dex than SLN (84 ± 5.4 vs 63 ± 3.2%) (Table 1).

Discussion

The goal of this work was to develop novel SLN to target inflammatory macrophages upon oral administration. To that purpose, the structure of nanoparticles should endure the GI transit; on the other hand, negatively charged nanoparticles would favor the tar-

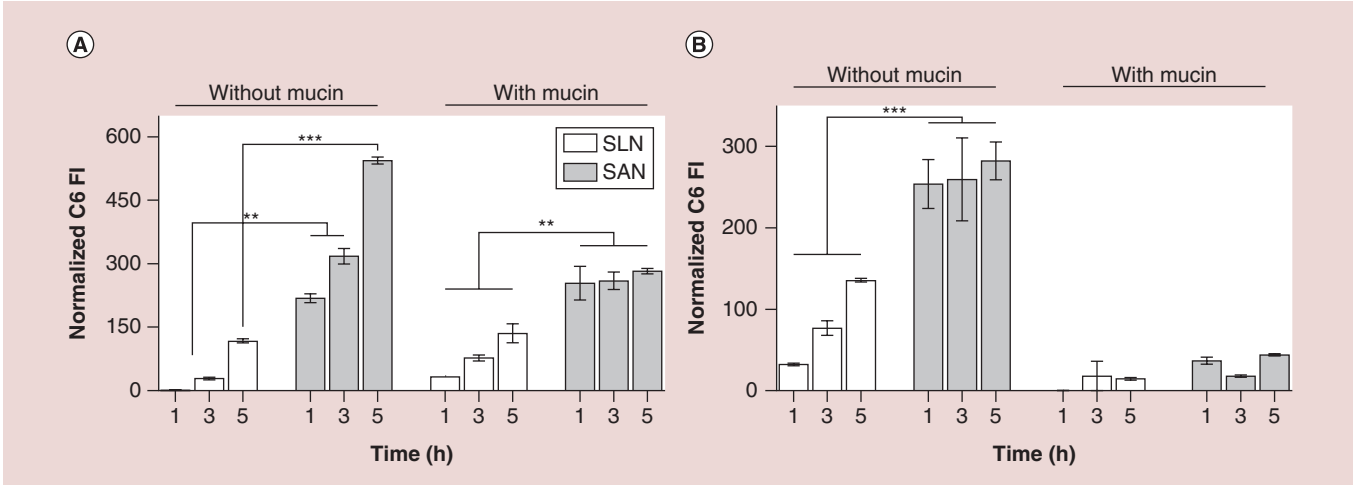

Figure 1. *In vitro* cellular uptake of nanoparticles. Normalized C6 fluorescence intensity (FI) of J774A.1 **(A)** and Caco-2 **(B)** cells after 1, 3 and 5 h of incubation with C6-labeled nanoparticles in the absence and presence of 0.5 mg/ml mucin. Values are expressed as mean ± SD (n = 3 batches).

geting to inflamed tissue via electrostatic interaction with positively charged proteins concentrated at the inflamed mucosa, avoiding its rapid elimination by diarrhea. Additionally, the nanoparticles size has to be small enough to penetrate the holes at the injured epithelium. Finally, after extensively uptaken by inflammatory macrophages, the carried anti-inflammatory dexamethasone has to be intracellularly released.

Active targeting strategies mediated by the presence of superficial ligands on nanoparticles, are central to achieve a selective drug delivery on target cells that express the corresponding receptors [38,39]. Active targeting however, is ordinarily administered by intravenous route, while the oral route is classically employed for different pharmaceutical forms of low molecular weight drugs. If orally administered, monoclonal antibodies or peptides used in active targeting are degraded in the acid medium of the stomach or by digestive enzymes. For instance, Mane and Muro [40] found that upon oral administration, 60% of the antibody anti-ICAM-1 dose (overexpressed in inflamed colon) bound to the surface of polystyrene nanoparticles was degraded, while the rest of the dose was deposited into the upper part of the GIT (stomach and duodenum). A similar outcome is expected for immunoliposomes decorated with anti-transferrin antibodies (the transferrin receptor is overexpressed in inflamed colon) that *ex vivo* showed to be highly adhesive to the inflamed mucosa [41]. Smaller nonprotein ligands, such as the sugars mannose and galactose, will probably be more structurally sound to the harsh environment of the GIT. The efficacy of nanoparticles decorated with

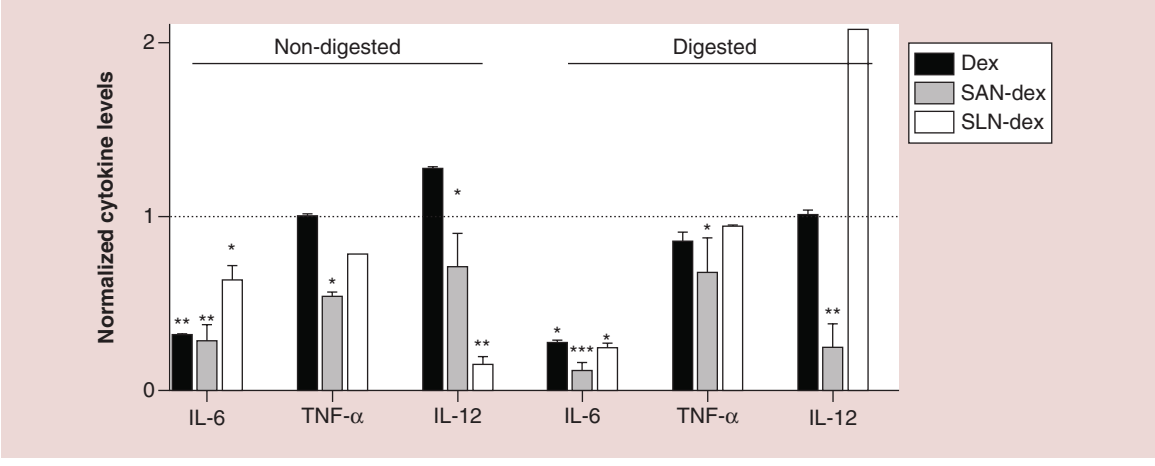

Figure 2. Inhibitory effect of non-digested and digested Dex-loaded nanoparticles on IL-6, TNF-α and IL-12 secretion from J774.A1 cells stimulated with 1 μg/ml lipopolysaccharides. Each cytokine level was normalized in respect to the level induced by lipopolysaccharide. Values are expressed by mean value ± S.D (n = 3) and analyzed using a one-way ANOVA compared with lipopolysaccharide.

mannose and galactose (to target the mannose receptor and the macrophage galactose-type lectin, highly expressed in activated macrophages, respectively) however, has only been tested *in vitro* [42,43].

On the other hand, the industrial production of surface decorated nanoparticles is challenging, due to the efficiency and reproducibility of coupling reactions that generally is not appropriate to be scaled-up, and the complex characterization required [44,45]. Therefore, manufacture strategies leading to nanoparticles of less complex structural features where proteins or peptides as surface ligands are replaced by other less prone to be destroyed by the oral route, are worth to be explored [46].

Having this in mind, we faced the preparation of new SLN, where the classical outer layer of phospholipid surfactant was replaced by the natural scavenger receptors class A ligand TPA, to further assess its structural properties. The TPA is a natural extract consisting in phosphatidylglycerophosphate methyl ester, sulphated diglycosyl diphytanylglycerol diether, phosphatidylglycerol (PG) and bisphosphatidyl glycerol [28]. Remarkably, preparing ultra-small SLN of size less than 100 nm is a true challenge, since nanoparticles tend to recrystallize in bigger sizes because of the lipidic nature of the core. Only recently, the successful production of ultra-small SLN has been reported [47–49]. Here, we found that upon replacing part of SPC by TPA, homogeneous ultra-small nanoparticles having significantly reduced size and negative Z potential were obtained. Surfactants play a fundamental role in the structural features of SLN. Surfactants reduce the surface tension of the emulsion, reducing the size and increasing the stability of the nanoparticles formed. Polyisoprenoid amphiphilic compounds, like TPA, with independence of the nature of the polar head groups, are better surfactants than phospholipids with linear acyl chains. Since aggregates of polyisoprenoid surfactants possess higher hydrophobicity than analogues of acyl chains, polyisoprenoids produce higher reduction on the superficial water tension than phospholipids (26–31 vs 41–46 mN/m, respectively) [50]. On the other hand, TPA are a mixture of lipids, where phosphatidylglycerophosphate methyl ester, the major component of the TPA and bisphosphatidyl glycerol, have two, and PG has one, phosphate groups negatively charged at physiological pH, respectively. The TPA is responsible for a strongly negative surface charge, a fact that leads to lower sized nanoparticles.

In a further step, negatively charged ultra-small SAN were shown to exhibit low interaction with mucins, as well as good mucus penetrating properties. Because of its TPA content, the uptake of SAN by J774A1 cells was sixfold higher than that of SLN. As a consequence of being more mucopentrating than SLN, the uptake of SAN occurred even across a thick mucin layer. The TPA content also protected SAN from pancreatic lipase degradation: while SLN and SAN were equally stable in SGF, the lipolysis of SAN was slower than that of SLN. Lipolysis is an interfacial process, where bile salts displace adsorbed molecules from the lipid-water interface before colipase and lipase are adsorbed [51]. Then, pancreatic lipase starts the hydrolysis of triglycerides into free fatty acids and monoglycerides. Phospholipids are rapidly displaced from interfaces by bile salts in the duodenum when phospholipid-stabilized emulsions are administered orally [52]. As bile salts tend to lie flat on that interface [53], it is more difficult for them to remove molecules that adsorb strongly to that interface and that occupy a high amount of its area [54]. The chain length and the surface area of surfactants are the principal factors that can delay or avoid lipolysis. Studies of archaeolipid monolayers have shown that phytanyl chains double the transversal area of that of acyl chains (100 A^2 vs 40–50 A^2) [50]. The combination of TPA strongly associated to the compritol core, with the high transversal area of archaeolipids in the interface could explain the inhibition of lipolysis by TPA. Finally, the presence of TPA in SAN was found to increase its colloidal stability and retention of Dex upon storage compared with SLN.

Dex loaded in SAN also induced the highest decrease of IL-6, TNF-α and IL-12 titers on J774A.1 cells stimulated with LPS as compared with free Dex and Dex loaded in SLN. Most importantly, the anti-inflammatory activity of SAN-Dex was retained after submitted to *in vitro* enzymatic digestion.

The importance of reducing proinflammatory cytokines in IBD, is evidenced by the great advance that the use of antibodies anti-TNF-α represented for Crohn's disease patients [55]. Cytokines not only induce intestinal inflammation and associated symptoms, such as diarrhea, but also regulate extra intestinal manifestations, such as arthralgia and arthritis, and systemic effects [56,57]. In addition, cytokines play a role in pathogenesis of the progressive and destructive forms of disease associated with intestinal stenosis, bleeding, abscess and fistula formations and cancer development [2,58]. TNF-α maintains chronic inflammation of the intestinal mucosa and it is implicated in development of arthritis and cachexia. IL-6 induces the release of acute phase proteins in the liver. In addition, blockage of signaling via IL-6 led to the improvement of a subgroup of patients with Crohn's disease [59]. Ustekinumab, a monoclonal antibody directed against the common p40 subunit of IL-12 and IL-23, is currently evaluated in Phase III studies [60].

Here we showed for the first time that SAN, produced by a simple mixture of TPA, Tween-80 and ordinary lipids in the absence of organic solvents, display higher structural endurance to the GIT agents than ordinary solid lipid nanoparticles, while expose targeting ligands that were refractory to chemical and enzymatic destruction, and that were included with no need for chemical derivatization. Oral targeted nanoparticles are still an emergent technology. Targeted delivery of anti-inflammatory drugs by the oral route aim to reduce their systemic availability and increase its local effect limiting it to the GIT, represent a more effective approach than the administration of free drugs in conventional pharmaceutical form.

Acknowledgements

The authors would like to thank MA de Farias and RV Portugal from the Electron Microscopy Laboratory, Brazilian Nanotechnology National Laboratory, for sample preparation and data acquisition of Cryo-TEM images.

Financial & competing interests disclosure

This work was supported by Secretaria de Investigaciones, Universidad Nacional de Quilmes. HE Jerez has a fellowship from National Council for Scientific and Technological Research (CONICET). HL Higa, EL Romero and MJ Morilla are members of the Research Career Program from CONICET. The authors have no other relevant affiliations or financial involvement with any organization or entity with a financial interest in or financial conflict with the subject matter or materials discussed in the manuscript apart from those disclosed.

No writing assistance was utilized in the production of this manuscript.

Summary points

Background

- Inflammatory bowel diseases such as Crohn's disease and ulcerative colitis, are incurable relapsing disorders of the GI tract, characterized by chronic inflammation and epithelial injury induced by the uncontrolled activation of the mucosal immune system.
- Delivering anti-inflammatory drugs to macrophages and dendritic cells with targeted nanoparticles could make inflammatory bowel disease treatments more efficient.

Results & discussion

- The formulation dexamethasone in solid archaeolipid nanoparticle (SAN) made of compritol as core and soybean phosphatidylcholine:total polar archaeolipids:Tween 80 as surface, were highly uptaken and induced the highest decrease of proinflammatory cytokines (IL-6, TNF-α and IL-12) on J774A.1 cells stimulated with lipopolysaccharides from *Escherichia coli* 0111:B4.
- After being submitted to *in vitro* digestion SAN-dexamethasone, but no ordinary solid lipid nanoparticles lacking total polar archaeolipids, retained the capacity to reduce the levels of proinflammatory cytokines.

Conclusion

- SAN, by merging high endurance against destructive agents in the GI tract with an extensive uptake by macrophages and negative charge surface, may be well suited for oral targeted delivery to the inflamed mucosa.

References

Papers of special note have been highlighted as: • of interest; •• of considerable interest

1 Danese S, Fiocchi C. Ulcerative colitis. *N. Engl. J. Med.* 365, 1713–1725 (2011).

2 Baumgart DC, Sandborn WJ. Crohn's disease. *Lancet* 380, 1590–1605 (2012).

3 Lewis RT, Maron DJ. Efficacy and complications of surgery for Crohn's disease. *Gastroenterol. Hepatol.* 6(9), 587–596 (2010).

4 Talley NJ, Abreu MT, Achkar JP *et al.* An evidence-based systematic review on medical therapies for inflammatory bowel disease. *Am. J. Gastroenterol.* 106(Suppl. 1), S2–S25 (2011).

5 Rutgeerts P, Vermeire S, Van Assche G. Biological therapies for inflammatory bowel diseases. *Gastroenterology* 136(4), 1182–1197(2009).

6 Gómez-Gómez GJ, Masedo A, Yela C, Martínez-Montiel M del P, Casís B. Current stage in inflammatory bowel disease: what is next? *World J. Gastroenterol.* 21(40), 11282–11303 (2015).

•• **Review of current treatments for inflammatory bowel diseases.**

7 Barnes PJ, Adcock IM. Glucocorticoid resistance in inflammatory diseases. *Lancet* 373(9678), 1915–1917 (2009).

8 Kopylov U, Ben-Horin S, Seidman E. Therapeutic drug monitoring in inflammatory bowel disease. *Ann. Gastroenterol.* 27, 304–312 (2014).

9 Ben-Horin S, Kopylov U, Chowers Y. Optimizing anti-TNF treatments in inflammatory bowel disease. *Autoimmun. Rev.* 13, 24–30 (2014).

10 Dave M, Purohit T, Razonable R, Loftus EV Jr. Opportunistic infections due to inflammatory bowel disease therapy. *Inflamm. Bowel Dis.* 20(1), 196–212 (2014).

11 Targownik LE, Bernstein CN. Infectious and malignant complications of TNF inhibitor therapy in IBD. *Am. J. Gastroenterol.* 108(12), 1835–1842 (2013).

12 Hua S, Marks E, Schneider JJ, Keely S. Advances in oral nano-delivery systems for colon targeted drug delivery in inflammatory bowel disease: selective targeting to diseased versus healthy tissue. *Nanomedicine* 11, 1117–1132 (2015).

•• **Review focused on what current nano-drug delivery systems can offer in overcoming the limitations of conventional drug formulations for the treatment of inflammatory bowel disease.**

13 Brennan FR, Dill Morton L, Spindeldreher S *et al.* Safety and immunotoxicity assessment of immunomodulatory monoclonal antibodies. *MAbs* 2(3), 233–255 (2010).

14 Heinsbroek Sigrid EM, Gordon S. The role of macrophages in inflammatory bowel diseases. *Expert Rev. Mol. Med.* 11, e14 (2009).

15 Neurath MF. Cytokines in inflammatory bowel disease. *Nat. Rev. Immunol.* 14(5), 329–342 (2014).

•• **Review on the role of cytokine and anticytokine therapies in inflammatory bowel disease.**

16 Antoni L, Nuding S, Wehkamp J, Stange EF. Intestinal barrier in inflammatory bowel disease. *World J. Gastroenterol.* 20(5), 1165–1179 (2014).

• **Review describing the components of the healthy intestinal mucosal barrier and their disturbances in inflammatory bowel disease.**

17 Tirosh B, Khatib N, Barenholz Y, Nissan A, Rubinstein A. Transferrin as a luminal target for negatively charged liposomes in the inflamed colonic mucosa. *Mol. Pharm.* 6, 1083–1091 (2009).

18 Canny G, Levy O, Furuta GT *et al.* Lipid mediator-induced expression of bactericidal/permeability-increasing protein (BPI) in human mucosal epithelia. *Proc. Natl Acad. Sci. USA* 99, 3902–3907 (2002).

19 Ramasundara M, Leach ST, Lemberg DA, Day AS. Defensins and inflammation: the role of defensins in inflammatory bowel disease. *J. Gastroenterol. Hepatol.* 24, 202–208 (2009).

20 Goggins BJ, Chaney C, Radford-Smith GL *et al.* Hypoxia and integrin-mediated epithelial restitution during mucosal inflammation. *Front. Immunol.* 11, 272 (2013).

21 Fallingborg J, Christensen LA, Jacobsen BA, Rasmussen SN. Very low intraluminal colonic pH in patients with active ulcerative colitis. *Dig. Dis. Sci.* 38(11), 1989–1993 (1993).

22 Lamprecht A, Schafer U, Lehr CM. Size-dependent bioadhesion of micro- and nanoparticulate carriers to the inflamed colonic mucosa. *Pharm. Res.* 18, 788–793 (2001).

• **First report that describes a size-dependent accumulation of nanoparticles specifically in the inflamed intestinal regions.**

23 Corcelli A, Lobasso S. Characterization of lipids of halophilic Archaea. *In: Methods in microbiology-extremophiles (volume 35).* Rainey AF, Oren AA (Eds). Elsevier, Amsterdam, The Netherlands, 585–613 (2006).

24 Altube MJ, Selzer SM, de Farias MA, Villares Portugal R, Morilla MJ, Romero EL. Surviv-ing nebulization-induced stress: dexamethasone in pH-sensitive archaeosomes. *Nanomedicine (Lond.)* 11(16), 2103–2117 (2016).

25 Gonzalez RO, Higa LH, Cutrullis RA *et al.* Archaeosomes made of *Halorubrum tebenquichense* total polar lipids: a new source of adjuvancy. *BMC Biotechnol.* 9, 71 (2008).

26 Kates M, Kushwaha SC. Isoprenoids and polar lipids of extreme halophiles. *In: Archaea: A Laboratory Manual, Halophiles.* Dassarma S (Ed.). Cold Spring Harbor Laboratory Press, NY, USA, 35–54 (1995).

27 Bötcher CJF, van Gent CM, Pries C. A rapid and sensitive submicron phosphorus determination. *Anal. Chim. Acta* 24, 203–204 (1961).

28 Higa LH, Schilrreff P, Perez AP *et al.* Ultradeformable archaeosomes as new topical adjuvants. *Nanomedicine* 8(8), 1319–1328 (2012).

29 Silva AC, González-Mira E, García ML *et al.* Preparation, characterization and biocompatibility studies on risperidone-loaded solid lipid nanoparticles (SLN): high pressure homogenization versus ultrasound. *Colloids Surf. B Biointerfaces* 86, 158–165 (2011).

30 Porter CJ, Charman WN. *In vitro* assessment of oral lipid based formulations. *Adv. Drug Deliv. Rev.* 50(Suppl. 1), S127–S147 (2001).

31 Serpe L, Canaparo R, Daperno M *et al.* Solid lipid nanoparticles as anti-inflammatory drug delivery system in a human inflammatory bowel disease whole-blood model. *Eur. J. Pharm. Sci.* 39, 428–436 (2010).

32 Petersen S, Steiniger F, Fischer D, Fahr A, Bunies H. The physical state of lipid nanopar-ticles influences their effect on in vitro cell viability. *Eur. J. Pharm. Biopharm.* 79, 150–161 (2011).

33 Jores K, Mehnert W, Drechsler M, Bunjes H, Johann C, Mäder K. Investigations on the structure of solid lipid nanoparticles (SLN) and oil-loaded solid lipid nanoparticles by photon correlation spectroscopy, field-flow fractionation and transmission electron microscopy. *J. Control. Release* 95(2), 217–227 (2014).

34 Kuntsche J, Horst JC, Bunjes H. Cryogenic transmission electron microscopy (cryo-TEM) for studying the morphology of colloidal drug delivery systems. *Int. J. Pharm.* 417, 120–137 (2011).

35 Fang J, Fang C, Liu C, Su Y. Lipid nanoparticles as vehicles for topical psoralen delivery: solid lipid nanoparticles (SLN) versus nanostructured lipid carriers (NLC). *Eur. J. Pharm. Biopharm.* 702, 633–640 (2008).

36 Yoon JJ, Kim JH, Park TG. Dexamethasone-releasing biodegradable polymer scaffolds fabricatedby a gas-foaming/salt-leaching method. *Biomaterials* 24, 2323–2329 (2004).

37 Griffiths PC, Cattoz B, Ibrahim MS, Anuonye JC. Probing the interaction of nanoparticles with mucin for drug delivery applications using dynamic light scattering. *Eur. J. Pharm. Biopharm.* 97A, 218–222 (2015).

38 Pakatip R, Cook JM, Florence AT. Nanosystem drug targeting: facing up to complex realities. *J. Control. Release* 141, 265–276 (2010).

39 Shapira A, Yoav DL, Henk JB, Assaraf YG. Nanomedicine for targeted cancer therapy: towards the

overcoming of drug resistance. *Drug Resist. Updat.* 14, 150–163 (2011).

40 Mane V, Muro S. Biodistribution and endocytosis of ICAM-1-targeting antibodies versus nanocarriers in the gastrointestinal tract in mice. *Int. J. Nanomedicine* 7, 4223–4237 (2012).

41 Harel E, Rubinstein A, Nissan A *et al.* Enhanced transferrin receptor expression by proinflammatory cytokines in enterocytes as a means for local delivery of drugs to inflamed gut mucosa. *PLoS ONE* 6(9), e24202 (2011).

42 Xiao B, Laroui H, Ayyadurai S *et al.* Mannosylated bioreducible nanoparticle-mediated macrophage-specific TNF-alpha RNA interference for IBD therapy. *Biomaterials* 34(30), 7471–7482 (2013).

43 Coco R, Plapied L, Pourcelle V *et al.* Drug delivery to inflamed colon by nanoparticles: comparison of different strategies. *Int. J. Pharm.* 440(1), 3–12 (2013).

44 Zhu S, Niu M, O'Mary H, Cui Z. Targeting of tumor associated macrophages made possible by PEG-sheddable, mannose modified nanoparticles. *Mol. Pharm.* 10(9), 3525–3530 (2013).

45 Zhao C, Fana T, Yang Y *et al.* Preparation, macrophages targeting delivery and anti-inflammatory study of penta-peptide grafted nanostructured lipid carriers. *Int. J. Pharm.* 450 (1–2), 11–20 (2013).

46 Hua S. Orally administered liposomal formulations for colon targeted drug delivery. *Front. Pharmacol.* 5, 138 (2014).

47 Schwarz JC, Baisaeng N, Hoppel M, Löw M, Keck CM, Valenta C. Ultra-small NLC for improved dermal delivery of coenyzme Q10. *Int. J. Pharm.* 447, 213–217 (2013).

48 Nafee N, Husari A, Maurer CK *et al.* Antibiotic-free nanotherapeutics: ultra-small, mucus-penetrating solid lipid nanoparticles enhance the pulmonary delivery and anti-virulence efficacy of novel quorum sensing inhibitors. *J. Control. Release* 192, 131–140 (2014).

49 Lohan SB, Bauersachs S, Ahlberg S *et al.* Ultra-small lipid nanoparticles promote the penetration of coenzyme Q10 in skin cells and counteract oxidative stress. *Eur. J Pharm. Biopharm.* 89, 201–207 (2015).

50 Yamauchi K, Onoue Y, Tsujimoto T, Kinoshita M. Archaebacterial lipids: high surface activity of polyisoprenoid surfactants in water. *Colloids Surf. B Biointerfaces* 10, 35–39 (1997).

51 Wickham M, Wilde P, Fillery-Travis A. A physicochemical investigation of two phosphatidylcholine/bile salt interfaces: implications for lipase activation. *Biochim. Biophys. Acta* 1580(2–3), 110–122 (2002).

52 Torcello-Gómez A, Maldonado-Valderrama J, de Vicente J, Cabrerizo-Vílchez MA, Gálvez-Ruiz MJ, Martín-Rodríguez A. Investigating the effect of surfactants on lipase interfacial behaviour in the presence of bile salts. *Food Hydrocolloids* 25, 809–816 (2011).

53 Maldonado-Valderrama J, Woodward NC, Gunning AP *et al.* Interfacial characterization of beta-lactoglobulin networks: displacement by bile salts. *Langmuir* 24(13), 6759–6767 (2008).

54 Wulff-Pérez M, de Vicente J, Martín-Rodríguez A, Gálvez-Ruiz MJ. Controlling lipolysis through steric surfactants: new insights on the controlled degradation of submicron emulsions after oral and intravenous administration. *Int. J. Pharm.* 423, 161–166 (2012).

55 van Dullemen HM, van Deventer SJ, Hommes DW *et al.* Treatment of Crohn's disease with anti-tumor necrosis factor chimeric monoclonal antibody (cA2). *Gastroenterology* 109, 129–135 (1995).

56 Strober W, Fuss IJ, Blumberg RS. The immunology of mucosal models of inflammation. *Annu. Rev. Immunol.* 20, 495–549 (2002).

57 Ruffolo C, Scarpa M, Faggian D *et al.* Subclinical intestinal inflammation in patients with Crohn's disease following bowel resection: a smoldering fire. *J. Gastrointestinal Surg.* 14, 24–31 (2010).

58 Peyrin-Biroulet L, Loftus EV Jr, Colombel J, Sandborn WJ. Long-term complications, extraintestinal manifestations, and mortality in adult Crohn's disease in population-based cohorts. *Inflamm. Bowel Dis.* 17, 471–478 (2011).

59 Ito H, Takazoe M, Fukuda Y *et al.* A pilot randomized trial of a human anti-interleukin-6 receptor monoclonal antibody in active Crohn's disease. *Gastroenterology* 126, 989–996 (2004).

60 Zundler S, Neurath MF. Interleukin-12: functional activities and implications for disease. *Cytokine Growth Factor Rev.* 26(5), 559–568 (2015).